GA–A24168

TESTS AND PERFORMANCE ON THE SIX GYROTRON SYSTEM ON THE DIII–D TOKAMAK

by

J. LOHR, Y.A. GORELOV, K. KAJIWARA, D. PONCE, R.W. CALLIS, J.R. FERRON, C.M. GREENFIELD, R.J. LA HAYE, R.I. PINSKER, R. PRATER, M.R. WADE, and R.A. ELLIS

SEPTEMBER 2002

DISCLAIMER

GA–A24168

TESTS AND PERFORMANCE ON THE SIX GYROTRON SYSTEM ON THE DIII–D TOKAMAK

by
J. LOHR, Y.A. GORELOV, K. KAJIWARA, D. PONCE, R.W. CALLIS, J.R. FERRON, C.M. GREENFIELD, R.J. LA HAYE, R.I. PINSKER, R. PRATER, M.R. WADE,† and R.A. ELLIS‡

This is a preprint of a paper presented at the 5th International Workshop on Strong Microwaves in Plasmas, August 1–9, 2002, Russia, and to be published in the *Proceedings.*

†Oak Ridge National Laboratory, Oak Ridge, Tennessee.
‡Princeton Plasma Physics Laboratory, Princeton, New Jersey.

Work supported by
U.S. Department of Energy under
Contracts DE-AC03-99ER54463, DE-AC05-00OR22725,
and DE-AC02-76CH03073

GENERAL ATOMICS PROJECT 30033
SEPTEMBER 2002

TESTS AND PERFORMANCE ON THE SIX GYROTRON SYSTEM ON THE DIII–D TOKAMAK

John Lohr, Y.A. Gorelov, K. Kajiwara, Dan Ponce, R.W. Callis, J.R. Ferron, C.M. Greenfield, R.J. LaHaye, R.I. Pinsker, R. Prater, M.R. Wade,† R.A. Ellis‡

General Atomics, P.O. Box 85608, San Diego, California, 92186-5608, USA
†Oak Ridge National Laboratory, Oak Ridge, Tennessee, 37831, USA
‡Princeton Plasma Physics Laboratory, Princeton New Jersey, USA

The DIII–D gyrotron complex for electron cyclotron heating (ECH) and electron cyclotron current drive (ECCD) has been expanded to include five operational gyrotrons with a sixth being commissioned. The generated rf power exceeds 4.0 MW and the transmission lines deliver about 80% of this power to the tokamak. Among the experiments performed during the most recent campaign, the installation has been used to achieve stabilization of the m/n=2/1 and 3/2 neoclassical tearing modes, to control the rate of current penetration early in the discharge, and to study ECCD contributions to advanced tokamak discharges with high bootstrap fractions. Observations of the thermal performance of CVD diamond output windows have shown good agreement with theoretical predictions, but have revealed a number of interesting phenomena connected with impurities, including points of visible light emission at hot spots identified by infrared measurements. One window was cleaned *in situ* by alumina grit blasting and Raman spectra verified the removal of some surface contamination. A significant new capability is the simultaneous control of the output power of the entire array of gyrotrons by the DIII-D plasma control system. This allows a predetermined electron temperature evolution to be followed at a specific location in the plasma and opens a new group of experimental possibilities leading to the achievement of higher levels of tokamak performance.

1. DIII–D ECH Installation

The DIII–D 110 GHz ECH installation comprises three Gycom* gyrotrons with 750 kW nominal output power and two second pulse length and two CPI** gyrotrons generating 1.0 MW for 5.0 s pulse length. A third CPI gyrotron opened a small leak through the copper of the collector and is currently being repaired. This tube has generated 550 kW for 10.0 s pulses and 800 kW for 0.7 s pulses. The power and pulse length performance of the system is summarized in Table 1.

The transmission lines are windowless and up to 100 m in length with up to 14 miter bends. In the worst case, the transmission efficiency is 80%, that is, the attenuation, measured in cold test, is –1 dB from the output of the matching optics unit (MOU) to beyond the final miter bend. The lines consist of evacuated 31.75 mm diameter circular corrugated waveguide and incorporate pairs of

Table 1. Power and pulse length parameters for the DIII–D ECH system

Gyrotron	Parameters			
	Current Best		Normal Operation	
	P_{GEN} (kW)	Length (s)	Power (kW)	Length (s)
Gycom 1 (Katya)	850	2.1	750	2.0
Gycom 2 (Boris)	750	2.1	750	2.0
Gycom 3 (Natasha)	650	2.1	650	2.0
CPI 1 (Scarecrow)	1000	0.8	in repair	at CPI
CPI 2 (Tin Man)	1000	5.0	800	5.0
CPI 3 (Lion)	1000	5.0	800	5.0

grooved mirrors providing flexible control of the elliptical polarization of the injected rf power. Monitors of the forward and reflected power, vacuum isolation and dummy load power measurements are also provided. Results of a cold test of line transmission are presented in Fig. 1. The source was swept over a 1% range to ensure that no resonances were present to bias the measurement. Transmission of the entire line was compared with short path transmission using the same hardware and a calibrated attenuator to provide the reference signal levels.

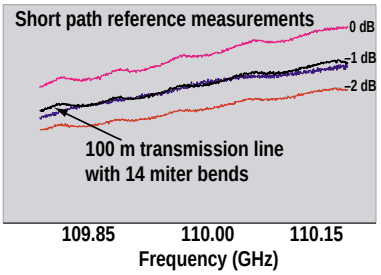

Fig. 1. Cold test measurements of the efficiency of a DIII-D transmission line 93 m in length having 14 miter bends, including two polarizing miters. The measured loss is –1 dB.

The polarization of the injected rf was measured by selecting linear polarization in two orthogonal directions at the final miter bend in the system and then making power measurements using orthogonal orientations of a fundamental rectangular horn and square law detector for signal picked off from the main beam with a –80 dB coupler. In all cases at least 95% of the rf power was in the desired polarization.

Coupling to the waveguide is performed for the Gycom gyrotrons using a two mirror phase correcting relay located in an evacuated MOU. This system has typically yielded 83%–85% efficiency. The two mirror system is necessary for these tubes to correct the intentionally broadened rf output beam to a free space Gaussian which couples well to the $HE_{1,1}$ waveguide mode for low loss transmission. The development of artificially grown diamond gyrotron output windows with $\tan(\delta)<1\times10^{-4}$ and thermal conductivity > 1.2 kW/m-K, has permitted gyrotrons to be designed which produce Gaussian rf beams directly without exceeding the maximum allowable power density in the center of the window. For these gyrotrons, a single ellipsoidal mirror can be used for

coupling. This arrangement, which has about 95% efficiency, reduces the cost of the coupling system. A comparison between the MOU power loading for the non-Gaussian two mirror system and the single mirror Gaussian system is shown in Fig. 2. The data are for the normal operating regimes of the gyrotrons and, although not normalized for the total power on any specific shot, the general increase in efficiency for the Gaussian beams is clear.

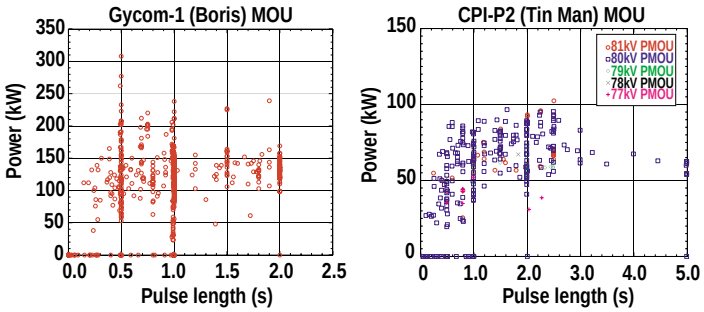

Fig. 2. MOU power loading for a two mirror phase correcting mirror system and a single mirror system coupling a Gaussian rf beam generated by a gyrotron with CVD diamond window to waveguide. The single mirror Gaussian coupler is nearly a factor of 3 more efficient than reconstruction of the Gaussian beam and coupling to waveguide with the two mirror system.

Each transmission line includes a combination dummy load which can be switched in remotely and used to absorb the rf power for tuning and monitoring. The first section of the combination is essentially a bad piece of waveguide in which a smooth wall section followed by tapered corrugations generates surface modes which are then damped evenly over a 1.5 m water cooled section. This portion of the load absorbs about 75% of the incident power and is cooled by water flow of about 4 ℓ/s. The remaining 25% of the power is absorbed by an inconel can load. The combination can handle 1 MW cw. Any power reflected from the inconel section is damped in the mode conversion section, therefore the two sections present an extremely black load for gyrotron testing. The loads are indistinguishable from the plasma from the standpoint of reflected rf power.

The rf beams are injected into the DIII–D tokamak from three articulating launcher assemblies, each of which can accommodate two rf beams. The launchers can scan over 40° in both the toroidal and poloidal directions and two of the launchers can scan at 10°/s in both directions. This range covers the maximum in co- and counter-current drive efficiency and the tokamak upper half plane poloidally.

The launchers are equipped with radiatively cooled mirrors having different designs for evaluation. The simplest have thin Glidcop mirrors held in an inconel frame. A modification to this design has a thicker region (boss)

in the center at the point of maximum power loading to provide thermal inertia. This mirror is grooved and oxidized on the back surface to enhance radiation to the water cooled shroud. For the launcher with the most delicate mirror drives, the mirrors are molybdenum brazed to graphite, minimizing the torque loading during disruptions. A fourth design uses a Glidcop mirror surface supported by a brazed multi-layer laminate of copper and inconel. This design has good thermal transfer away from the mirror surface with low eddy currents during disruptions. The bossed and laminated mirrors are designed for 1 MW 10–second pulses.

2. CVD Diamond Windows

The CVD diamond windows on the DIII–D CPI gyrotrons have been characterized. For about 800 kW passing through the windows, the peak central temperatures on two of the windows, measured using an infrared camera, plateau after about 3 s at values consistent with ANSYS modeling which maintains a factor of about three below the yield stress of 350 MPa. The third window, installed on the CPI-P1 (Scarecrow) gyrotron, has a time dependence of temperature after a 700 ms pulse indicating that its peak temperature could equilibrate after reaching a dangerously high value in excess of 200°C. These results are summarized in Fig. 3. In order to perform the measurements, the emissivity of the diamond was measured in a test setup simulating the actual installation. The camera can see the inside of the gyrotron through the window, which makes a measured 10% maximum contribution to the window measurement. Typically the effective emissivity is found to be about 0.1 for clean diamond viewed through a room temperature sapphire window in the test setup. But any contamination on the window surface could invalidate the calibration and the modeling by increasing the absorbed power for a given tan(δ) of the bulk material or by increasing the emissivity or both. Once the window is installed on the gyrotron, contamination on the inside surface is inaccessible for evaluation or cleaning. The CPI-P1 gyrotron developed a small vacuum leak through the copper of the collector, which is being repaired. The cleanliness of the window will be evaluated during the course of the repair.

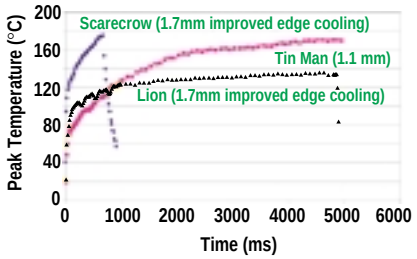

Fig. 3. Peak central temperature of the CVD diamond windows on the three CPI gyrotrons. Two of the windows have performance consistent with the modeling calculations, while one has abnormally high apparent temperature for 700 ms pulses. This could be due to a coating resulting in unexpectedly high microwave absorption, to emissivity higher than the calibrated value or both.

The window on the CPI-P2 (Tin Man) gyrotron was suspected to have been coated during the braze and bakeout processes and the outer surface was cleaned

by blasting with 3 μm diameter alumina grit. Raman scattering measurements performed *in situ* before and after the cleaning indicated that outer surface contamination was removed by this process.

On all the diamond windows bright spots are observed both in the visible and infrared during high power operation. These are assumed to be small particulate contamination on the window surface which is heated by the beam. Infrared hot spots which are not seen in the visible view could be impurities, probably graphite, in the bulk of the window lattices. Because the DIII–D system operates in vacuum, there is no tendency for the surface particulates to be burned away during high power operation. The very high thermal conductivity of the diamond appears to obviate excessive stress buildup from these local hot spots. As with the bulk measurements of window temperature, it is difficult to differentiate between areas of higher than ambient temperature and areas with higher emissivity. The apparent temperatures measured by infrared techniques therefore represent the upper bound on the inferred temperatures.

3. Feedback Control of the Generated rf Power

The DIII–D Plasma Control System (PCS) has been used to modulate the total rf power generated by the gyrotrons in response to a pre-programmed requirement. Although this new capability is still in the demonstration stage, no difficulties or instabilities in the control process have been identified.

In the first tests of the capability, a desired time evolution of the electron temperature at an intermediate radius in the plasma was programmed into the PCS. The electron temperature measured by the ECE diagnostic was compared with the pre-programmed waveform and an error signal was generated, which was converted to a command to the ECH complex to generate higher or lower power as required to zero the error signal. The gyrotrons can be modulated from 100% to about 10% of maximum output by changing the applied high voltage from the nominal operating value to about 80% of nominal, the exact range having been determined by the operators so that the output remains a monotonic function of applied high voltage. In Fig. 4(a) the results of a test are presented in which a sawtooth time dependence of the electron temperature at a normalized radius $\rho=0.4$ was commanded. The actual temperature was measured by the ECE diagnostic and the gyrotron complex was modulated accordingly to bring the command and the measurement together.

Limitations on the fidelity with which the temperature tracks the command arise due to the finite injected rf power, the inability to decrease the temperature faster than about an energy confinement time and the necessity of maintaining some minimum rf output to ensure clean response when a power increase is required. The capability was then used to demonstrate that the flux penetration early in a plasma discharge could be controlled by controlling the electron

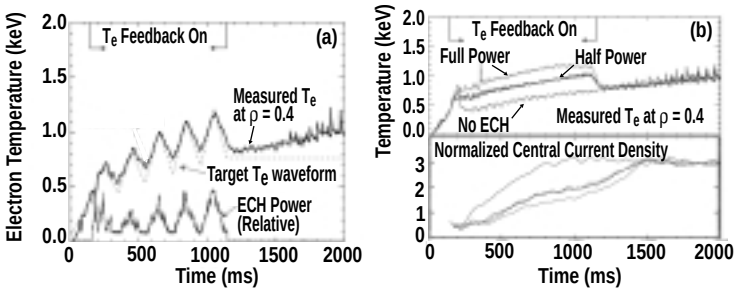

Fig. 4. (a) Test of PCS feedback control of the ECH system power. The target temperature was preprogrammed and compared with ECE measurements. The difference signal then determined the modulator output. (b) The PCS feedback control was then used to control T_e and determine the rate of flux penetration early in the discharge.

temperature. In Fig. 4(b) the central current density measured by the MSE diagnostic is plotted as a function of time for a series of four discharges in which different time evolutions of the electron temperature at ρ=0.4 were commanded. The lowest temperature case was for no rf injection and the electron temperature evolved normally. The two intermediate temperature cases had a pre-programmed temperature evolution and indicate the excellent reproducibility. The highest temperature case used nearly the maximum available rf output power. At the highest electron temperature, the flux penetration is slowed and the central current density increases more slowly. The case without rf has the most rapid flux penetration and the two cases with intermediate power lie in between the extremes. In the future, active control of both the steering and the power of the injected rf will be used to facilitate other experiments with demanding requirements for reproducibility and profile control.

4. Experimental Results

4.1. Neoclassical Tearing Mode Suppression

The neoclassical tearing mode (NTM) manifests itself as a helical tube following a low order rational magnetic field line which has less than the ambient current density. The mode typically is triggered by a transient MHD event, for example a sawtooth crash, which forms an island in the normally concentric flux surfaces responsible for good tokamak confinement. Within the island, once it forms, the electron temperature is nearly constant as a function of plasma radius, with the result that the pressure gradient driven bootstrap current within the island drops to zero. The island is a stable structure, which can lock to the vessel wall stopping plasma rotation and precipitating a disruptive termination. Across the width of the island transport is rapid, so even if the island does not precede a disruption, confinement is degraded and the plasma beta decreases. The instability can be stabilized by electron cyclotron current

drive which is applied to the interior of the island structure. The island width is typically about 8 cm in DIII–D and the DIII–D ECH system, which can drive current in a region extending about 6 cm radially and 8–10 cm poloidally and toroidally is well suited to generate current within the necessary localized volume. The current required for stabilization is moderate, about the value of the absent bootstrap current in the island, 100–200 kA.

The ECH system has been able to stabilize both the m/n=3/2 and 2/1 tearing modes on DIII–D. The ECCD must be located to within about 2 cm of the island center to achieve stabilization. The exact location at which to drive current can be determined empirically by scanning the ECCD region across the island. In Fig. 5 two discharges are shown in which the m/n=3/2 NTM was targeted. In the first, the toroidal magnetic field was scanned under control of the PCS and the amplitude of the NTM was measured by magnetic probes connected to observe even n modes. As the field changed, the $2\omega_{ce}$ resonance and ECCD location was swept across the pre-existing island structure. At a particular value of B_T, a decrease in the mode amplitude was noted. On a subsequent discharge, the toroidal field was maintained at that value and the mode was stabilized. Following stabilization, in the absence of a seed island, it was possible to increase β above the previous value at which the NTM had occurred.

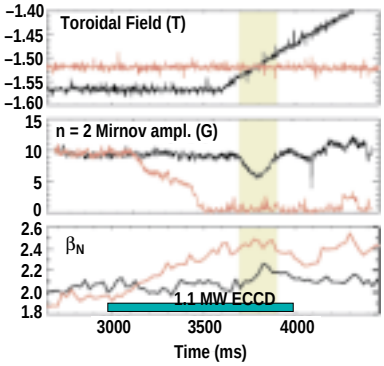

Fig. 5. Suppression of the m/n=3/2 tearing mode by ECCD. The ECCD location was determined by sweeping the resonance past the islands by varying B_T.

The m/n=2/1 NTM is more difficult to stabilize, since it lies at a larger radius than the 3/2 mode and has a smaller width. This mode often precedes a disruption, so for large future devices like ITER, which could suffer damage in a major disruption, its stabilization is of some importance. Stabilization of this mode has also been demonstrated, as shown in Fig. 6. The PCS commanded a decrease in β once the mode had been started to make it easier to stabilize with the limited rf power, about 2.2 MW, available. The control system then varied B_T by moving the resonance ≈2 cm to achieve stabilization. Although a direct on/off comparison was not performed, on a comparison shot with the same β program, for which the ECCD was not at the island location, the mode persisted.

4.2. ECCD Efficiency

It is critical, both for NTM suppression and for advanced tokamak operation with non-monotonic j(r) profiles, that the efficiency of ECCD not decrease

as the ECCD location is moved. The efficiency is expected to decrease as the local electron temperature decreases, that is, as the current drive is moved out from the plasma center. It also is expected that increasing the perpendicular component (to the magnetic field) of the electron velocity increases trapping of the heated electrons, removing a fraction of the population from the role of current carrier and decreasing the current drive efficiency. It was found through detailed efficiency measurements that, for high enough values of β, the current drive efficiency remained high even if the resonance were moved outside the magnetic axis to the banana region as shown in Fig. 7.

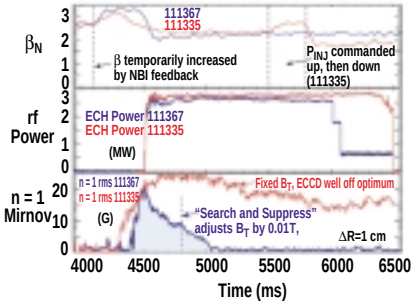

Fig. 6. Suppression of the m/n=2/1 tearing mode by ECCD. For the comparison without suppression, the ECCD was applied away from the islands.

This observation, which makes ECCD even more attractive for MHD suppression and advanced tokamak operation, can be explained by a shift of the resonant electrons away from the trapping boundary as β increases.

Up to 140 kA of EC driven current has been observed in DIII–D for injected rf power to about 2 MW. This efficiency is sufficient both for advanced tokamak scenarios currently under consideration and for MHD mode suppression, as described above.

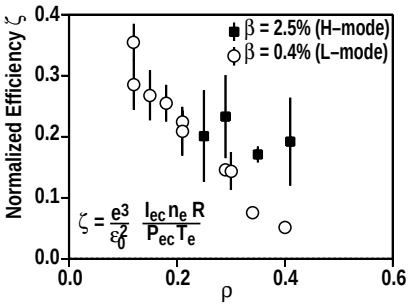

Fig. 7. The ECCD efficiency remains high for off-axis absorption if β remains high.

5. Conclusion

The 110 GHz ECH/ECCD system on the DIII–D tokamak generates in excess of 4 MW for pulse lengths greater than 2 s, with about 1.6 MW available for 5 s pulses. Experiments have been performed on MHD suppression, feedback control of the output power and ECH and ECCD efficiency.

Acknowledgment

Work supported by U.S. Department of Energy under Contracts DE-AC03-99ER54463, DE-AC05-00OR22725, and DE-AC02-76CH03073.

*Gycom, Nizhny, Novgorod, Russia.

**Communications and Power Industries, Palo Alto, California, USA.